Electronic Supporting Information for

Metal-organic layer derived metal hydroxide nanosheets for highly efficient oxygen evolution

Wen-Da Zhang,‡[a] Xiaodong Yan,‡[a] Tao Li,[a] Yong Liu,[a] Qiu-Ting Fu,[a] and Zhi-Guo Gu*[a,b]

[a]*Key Laboratory of Synthetic and Biological Colloids,Ministry of Education, School of Chemical and Material Engineering, Jiangnan University, Wuxi 214122, P.R.China.*
[b]*International Joint Research Center for Photoresponsive Molecules and Materials, School of Chemical and Material Engineering, Jiangnan University, Wuxi 214122, P.R. China.*
‡ These authors contributed equally to this work.

E-mail: zhiguogu@jiangnan.edu.cn

Table of contents

1. Experimental Section

All reagents and solvents were purchased from commercial sources and used without further purification. $MnCl_2 \cdot 4H_2O$, $FeCl_2 \cdot 4H_2O$, $CoCl_2 \cdot 6H_2O$, $NiCl_2 \cdot 6H_2O$, CH_3CH_2OH and KOH were purchased from SINOPHARM GROUP Co., ltd. Iridium(IV) dioxide (IrO_2) was purchased from Alfa Aesar. Nafion and $K_2[Ni(CN)_4] \cdot 3H_2O$ were purchased from Sigma-Aldrich. Ni foam with a thickness of 2 mm was purchased from Suzhou Wingrise Energy Technology Co., ltd.

Infrared spectra were recorded on an ABB Bomem FTLA 2000-104 spectrometer with KBr pellets in the region of 500−4000 cm^{-1}. The powder X-ray diffraction data were collected on Bruker D8 Venture diffractometers using Cu Kα radiation sources (λ = 1.54178 Å). Electron microscopy images were collected on a Hitachi S-4800 and JEOL 2100 High Resolution Transmission Electron Microscopy. Atomic Force Microscope (AFM) for morphology studies were collected using Bruker MultiMode 8. The crystal structures were determined on a Siemens (Bruker) SMART CCD diffractometer using monochromated Mo $K\alpha$ radiation (λ = 0.71073 Å). Cell parameters were retrieved using SMART software and refined using SAINT[1] on all observed reflections. The highly redundant data sets were reduced using SAINT[1] and corrected for Lorentz and polarization effects. Absorption corrections were applied using SADABS[2] supplied by Bruker. Structures were solved by direct methods using the program SHELXL-97[3]. All the non-hydrogen atoms were refined with anisotropic thermal displacement coefficients. Hydrogen atoms were located geometrically and refined in a riding model. X-ray photoelectron spectroscopy measurements were carried out with an AXIS Supra by Kratos Analytical Inc. using monochromatized Al Ka radiation (hv = 1486.6 eV, 225 W) as X-ray source with a base pressure of 10^{-9} torr. Survey scan spectra were acquired using a pass energy of 160 eV and a 1 eV step size. Narrow region scans were acquired using a pass energy of 40 eV and a 0.1 eV step size. The hybrid lens mode was used in both cases. The analyzed area of all XPS spectra was 300 × 700 μm^2. A charge neutralizer was used throughout as the samples were mounted such that they were electrically isolated from the sample bar. All spectrums were calibrated by C 1s (284.8 eV).

2. Synthesis of 2D Hofmann-type MOF

Preparation of bulk $Mn(H_2O)_2Ni(CN)_4 \cdot 4H_2O$

In a 20 mL test tube, a mixture of CH_3CH_2OH and H_2O (v/v, 1:1, 8 mL) was gently layered on the top of a 2 mL water solution of $K_2[Ni(CN)_4] \cdot 3H_2O$ (11.80 mg, 0.04 mmol). A solution of $MnCl_2 \cdot 4H_2O$ (7.91 mg, 0.04 mmol) in 2 mL of CH_3CH_2OH was added carefully as a third layer. After three weeks, colorless block-shaped crystals of $Mn(H_2O)_2Ni(CN)_4 \cdot 4H_2O$ were collected, then washed with H_2O and dried in atmosphere. Yield: 30%. Anal. Calcd for $C_4H_{12}MnN_4NiO_6$: C, 14.74; H, 3.71 N, 17.19. Found: C, 14.82; H, 3.89 N, 16.92. IR (KBr, νcm^{-1}, Fig. S1a): 1627, 2150, 3265, 3611.

Preparation of bulk $Fe(H_2O)_2Ni(CN)_4 \cdot 4H_2O$

In a 20 mL test tube, a mixture of CH_3CH_2OH and H_2O (v/v, 1:1, 8 mL) was gently layered on the top of a 2 mL water solution of $K_2[Ni(CN)_4] \cdot 3H_2O$ (11.80 mg, 0.04 mmol). A solution of $FeCl_2 \cdot 4H_2O$ (7.95 mg, 0.04 mmol) in 2 mL of CH_3CH_2OH was added carefully as a third layer. After three weeks, light yellow block-shaped crystals of $Fe(H_2O)_2Ni(CN)_4 \cdot 4H_2O$ were collected, then washed with H_2O and dried in atmosphere. Yield: 45%. Anal. Calcd for $C_4H_{12}FeN_4NiO_6$: C, 14.71; H, 3.70 N, 17.14. Found: C, 14.82; H, 3.85; N, 16.83. IR (KBr, νcm^{-1}, Fig. S1b): 1613, 2160, 3599.

Preparation of bulk $Co(H_2O)_2Ni(CN)_4 \cdot 4H_2O$

In a 20 mL test tube, a mixture of CH_3CH_2OH and H_2O (v/v, 1:1, 8 mL) was gently layered on the top of a 2 mL water solution of $K_2[Ni(CN)_4] \cdot 3H_2O$ (11.80 mg, 0.04 mmol). A solution of $CoCl_2 \cdot 6H_2O$ (9.52mg, 0.04 mmol) in 2 mL of CH_3CH_2OH was added carefully as a third layer. After three weeks, pink block-shaped crystals of $Co(H_2O)_2Ni(CN)_4 \cdot 4H_2O$ were collected, then washed with H_2O and dried in atmosphere. Yield: 35%. Anal. Calcd for $C_4H_{12}CoN_4NiO_6$: C, 14.57; H, 3.67 N, 16.99. Found: C, 14.63; H, 3.85 N, 16.83. IR (KBr, νcm^{-1}, Fig. S1c): 1615, 2163, 3599.

Preparation of bulk $Ni(H_2O)_2Ni(CN)_4 \cdot 4H_2O$

In a 20 mL test tube, a mixture of CH_3CH_2OH and H_2O (v/v, 1:1, 8 mL) was gently

layered on the top of a 2 mL water solution of $K_2[Ni(CN)_4]\cdot 3H_2O$ (11.80 mg, 0.04 mmol). A solution of $NiCl_2\cdot 6H_2O$ (9.51 mg, 0.04 mmol) in 2 mL of CH_3CH_2OH was added carefully as a third layer. After three weeks, green block-shaped crystals of $Ni(H_2O)_2Ni(CN)_4\cdot 4H_2O$ were collected, then washed with H_2O and dried in atmosphere. Yield: 40%. Anal. Calcd for $C_4H_{12}N_4Ni_2O_6$: C, 14.58; H, 3.67 N, 17.00. Found: C, 14.62; H, 3.78 N, 17.12. IR (KBr, νcm^{-1}, Fig. S1d): 1616, 2164, 3207, 3609.

3. Preparation of $M(H_2O)_2Ni(CN)_4$ (M = Mn, Fe, Co, Ni) MOL

In a typical experiment, 10 mg of bulk Mn-MOF were dispersed in 20 mL ethanol. The mixture was sonicated for 120 min. The resulting suspension was centrifuged at 2000 rpm for 3 min to remove the unexfoliated bulk Mn-MOF. Then the upper suspension was sonicated for 120 min again. The ultrathin nanosheets Mn-MOL (the upper solution) were separated through high speed centrifugation (8000r), which were used for characterization of various electron microscope tests directly. Yield: 25%. IR (KBr, νcm^{-1}, Fig. S1a): 1620, 2142, 3258, 3620. Fe-MOL, Co-MOL and Ni-MOL were obtained by adopting the same synthetic procedures. For Fe-MOL, Yield: 20%. IR (KBr, νcm^{-1}, Fig. S1b): 1618, 2155, 3588. For Co-MOL, Yield: 20%. IR (KBr, νcm^{-1}, Fig. S1c): 1612, 2158, 3595. For Ni-MOL, Yield:15%. IR (KBr, νcm^{-1}, Fig. S1d): 1613, 2162, 3202, 3605.

4. Preparation of $M(OH)_X$ (M = Mn, Fe, Co, Ni) nanosheets

10 mg of MOL were dispersed in 20 mL water, and the mixture was sonicated for 60 min to ensure complete dispersion. Then 0.1 M potassium hydroxide solution was added dropwise until the color of solution no longer changed. The crude product was then obtained by centrifugation, then washed several times with water and ethanol. The samples were dried overnight in an oven at 40 ℃. For $Mn(OH)_2$, Yield: 35%. IR (KBr, νcm^{-1}, Fig. S4): 3410, 3060, 1583; For $Fe(OH)_3$, Yield: 40%. IR (KBr, νcm^{-1}, Fig. S4): 3450, 3000, 1654; For $Co(OH)_2$, Yield:35%. IR (KBr, νcm^{-1}, Fig. S4): 3660, 3420, 1590, 1372; For $Ni(OH)_2$, Yield: 25%. IR (KBr, νcm^{-1}, Fig. S4): 3653, 3450, 1384.

5. Electrochemical Characterization

Electrochemical measurements of all samples ($Mn(OH)_2$-NS, $Fe(OH)_3$-NS, $Co(OH)_2$-NS, $Ni(OH)_2$-NS, and IrO_2) were performed under the same conditions. Catalytic behaviors of the working electrodes were evaluated by a CHI 760E electrochemical workstation. Ni foam loaded with catalysts was used as the working electrode (its geometric surface area is 1 cm^2), while a platinum plate and a Hg/HgO electrode were used as the counter electrode and reference electrodes respectively. All the electrochemical measurements were taken in O_2-saturated KOH solutions. Before collecting the data, the catalysts were run for 10 cycles for activation. Typically, 2 mg of electrocatalyst powder was dispersed in 0.48 mL of 1:1 (V/V) DI water/EtOH mix solvent with 20 μL Nafion solution. The mixture was sonicated for about 1 hour to form a homogeneous catalyst ink. 40μL of the ink was attached on the Ni foam and dried in oven for 12 h. The mass loading on each electrode is about 0.16 mg cm^{-2}. Linear sweep voltammogram (LSV) was obtained at the scan rate of 5 mV s^{-1} in 1 M KOH. Tafel slopes were derived from the LSV curves. Chronopotentiometric measurements were conducted for the stability research at the current density of 10 mA cm^{-2} over 50 h. Electrochemical impedance spectroscopy (EIS) was collected at 1.52 V versus RHE in the frequency range of 0.01−10^6 Hz by applying an amplitude of 10 mV. To calculate the ECSA, the electrochemical double layer capacitance (EDLC) of the working electrode was obtained by virtue of CV curves at different scan rates. The EDLC was calculated by plotting the scan rate vs. current density difference at a certain potential. The IrO_2 electrode was prepared as follows. 2 mg of electrocatalyst powder was dispersed in 0.48 mL of 1:1 (V/V) DI water/EtOH mix solvent with 20 μL of Nafion solution. The mixture was sonicated for about 1 h to form a homogeneous catalyst ink. Then 40 μL of the ink was attached on the Ni foam and dried in oven for 12 h. The mass loading is about 0.16 mg cm^{-2}. The potential was converted according to the equation: $E_{RHE} = E_{Hg/Hgo} + 0.098 + 0.059 \times pH = E_{Hg/Hgo} + 0.924$. The overpotential was computed as: $\eta = E_{RHE} - 1.23$ V. The turnover frequency (TOF) value is calculated from the equation: $TOF = \frac{JA}{4Fn}$. Where J is the measured current density at the overpotential of 0.3 V, A is the surface area of the working electrode, F is the Faraday constant (96485 c/mol), and n is the number of moles of active materials loaded on the electrodes.

6. Table S1. Summary of crystallographic data for Mn-MOF and Co-MOF

	Mn-MOF	Co-MOF
Formula	$C_4H_{12}MnN_4NiO_6$	$C_4H_{12}CoN_4NiO_6$
Fw	325.83	329.82
T (K)	173(2)	173(2)
λ (Å)	0.71073	0.71073
Crystal system	Orthorhombic	Orthorhombic
Space group	*Pnma*	*Pnma*
a (Å)	12.1445(9)	12.0628(12)
b (Å)	14.1014(12)	13.8833(9)
c (Å)	7.311(5)	7.1686(5)
α (°)	90	90
β (°)	90	90
γ (°)	90	90
V (Å^3)	1252(17)	1200(17)
Z	4	4
D_{calc} (Mg/m^3)	1.729	1.825
μ (mm^{-1})	2.53	2.97
F(000)	660	668
θ (°)	3.1-25.4	2.9-26.4
Index ranges	$-14 \le h \le 13$ $-16 \le k \le 16$ $-8 \le l \le 8$	$-14 \le h \le 13$ $-17 \le k \le 17$ $-8 \le l \le 8$
Reflections collected	5588	2768
GOF (F^2)	1.00	1.04
$R_1{}^a$,$wR_2{}^b$($I>2\sigma(I)$)	0.064, 0.603	0.075, 0.626
$R_1{}^a$,$wR_2{}^b$(all data)	0.034, 0.066	0.03, 0.058

$R_1{}^a = \Sigma||F_o| - |F_c||/\Sigma F_o|$. $wR_2{}^b = [\Sigma w(F_o{}^2 - F_c{}^2)^2/\Sigma w(F_o{}^2)]^{1/2}$

7. Table S2. Selected bond lengths [Å] and angles [°] for Mn-MOF and Co-MOF

Mn-MOF		Co-MOF	
Ni1—C1	1.867 (3)	Ni1—C1	1.865 (3)
Ni1—C1^{i}	1.867 (3)	Ni1—C2	1.863 (3)
Ni1—C2^{i}	1.864 (3)	Ni1—C2^{v}	1.863 (3)
Ni1—C2	1.864 (3)	Ni1—C1^{v}	1.865 (3)
Mn2—N1	2.197 (3)	Co1—N2^{i}	2.095 (2)
Mn2—N1^{ii}	2.197 (3)	Co1—N2^{ii}	2.095 (2)
Mn2—N2^{iii}	2.201 (3)	Co1—N1^{iii}	2.103 (2)
Mn2—N2^{iv}	2.201 (3)	Co1—N1	2.103 (2)
Mn2^{v}— N2	2.201 (3)	Co1^{iv}—N2	2.095 (2)
C1—N1	1.144 (4)	C1—N1	1.147 (3)
C2—N2	1.147 (4)	C2—N2	1.149 (3)
N2^{iii}—Mn2—O1^{ii}	92.44 (9)	N2^{i}—Co1—N1^{iii}	90.38 (8)
N2^{iv}—Mn2—O1^{ii}	87.56 (9)	N2^{ii}—Co1—N1	89.62 (8)

Symmetry codes for Mn-MOF: (i) x, −y+1/2, z; (ii) −x+1, −y+1, −z+1; (iii) −x+1, −y+1, −z+2; (iv) x, y, z−1; (v) x, y, z+1.

Symmetry codes for Co-MOF: (i) −x, −y+1, −z+1; (ii) x, y, z−1; (iii) −x, −y+1, −z; (iv) x, y, z+1; (v) x, −y+1/2, z.

8. XRD patterns of 2D MOF

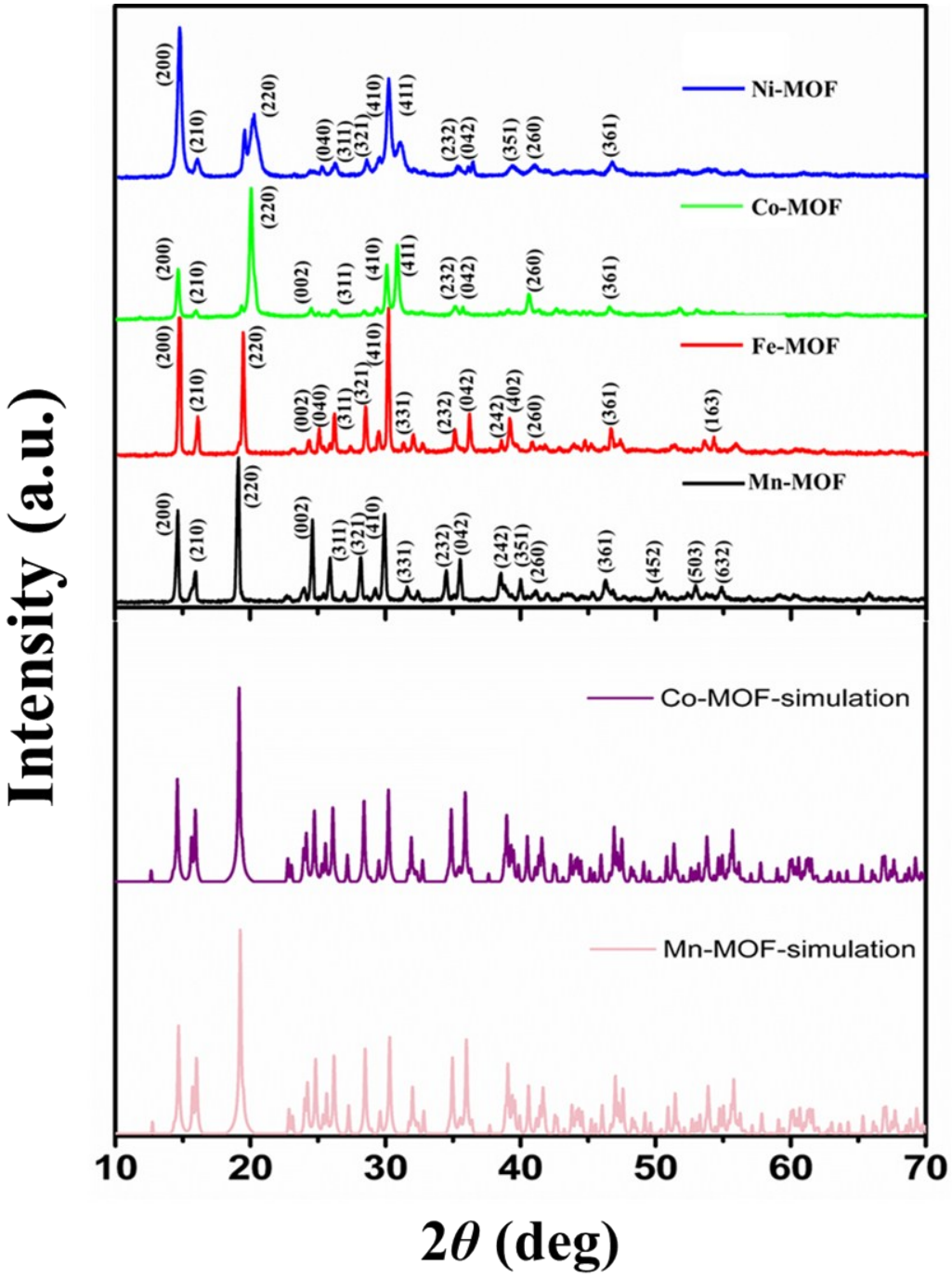

Fig. S1 XRD pattern of Mn-MOF, Fe-MOF, Co-MOF, Ni-MOF, Co-MOF-simulation and Mn-MOF-simulation.

9. SEM images of 2D Hofmann-type MOF

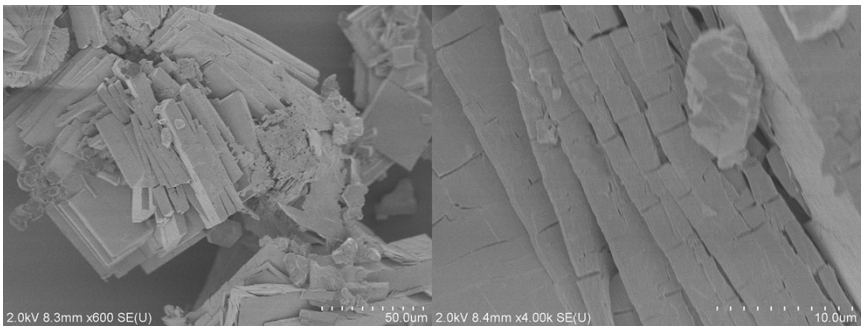

Fig. S2 SEM images of Mn-MOF.

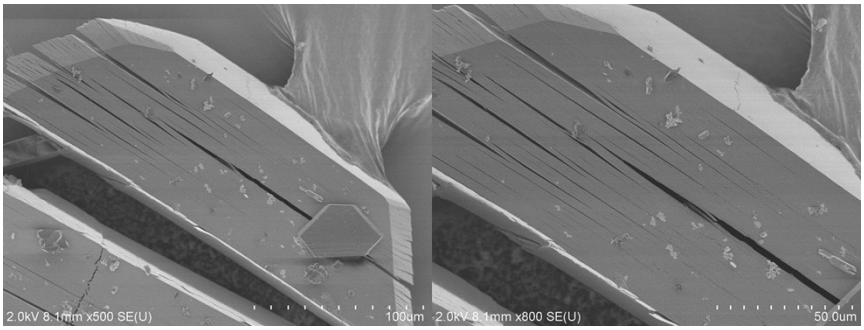

Fig. S3 SEM images of Fe-MOF.

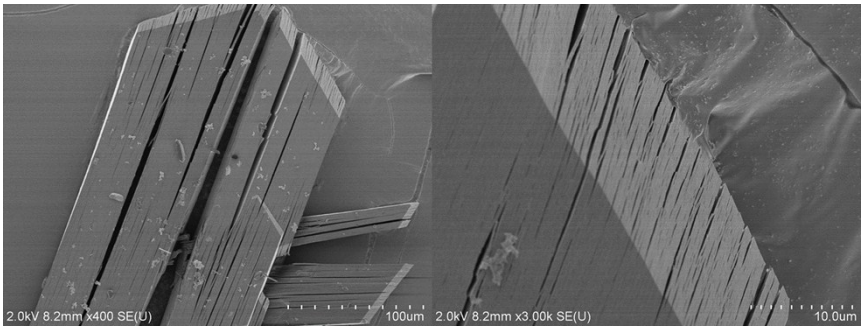

Fig. S4 SEM images of Co-MOF.

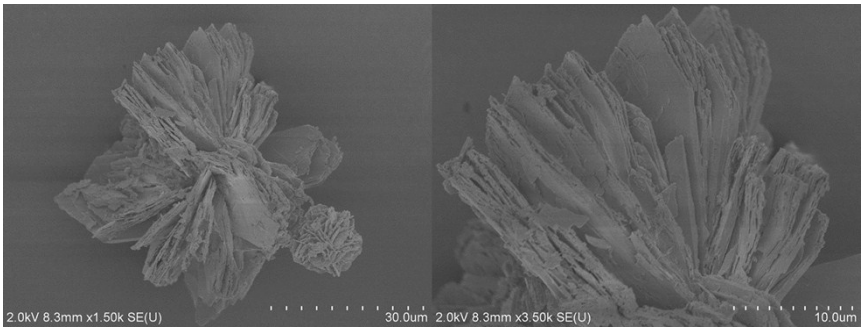

Fig. S5 SEM images of Ni-MOF.

10. Tyndall effect of Fe-MOL

Fig. S6 Tyndall effect (left) before and (right) after exfoliation.

11. TEM and SEM images of M-MOL

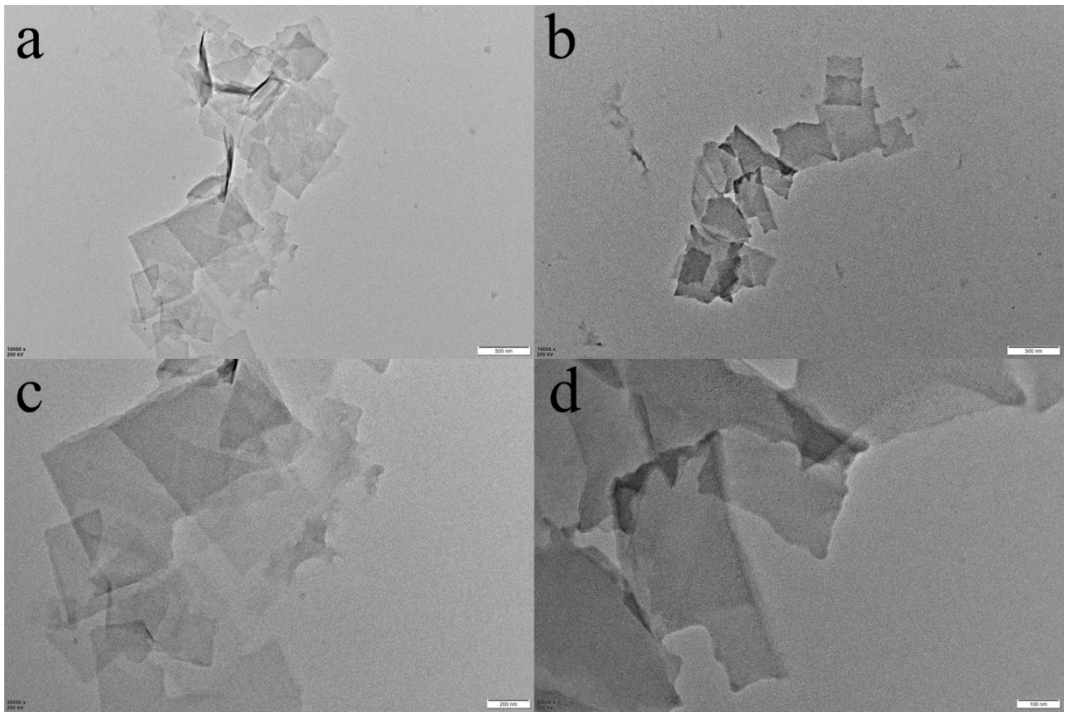

Fig. S7 TEM images of Mn-MOL (Scale bar: (a)500 nm, (b)500 nm, (c)200 nm, (d)100 nm).

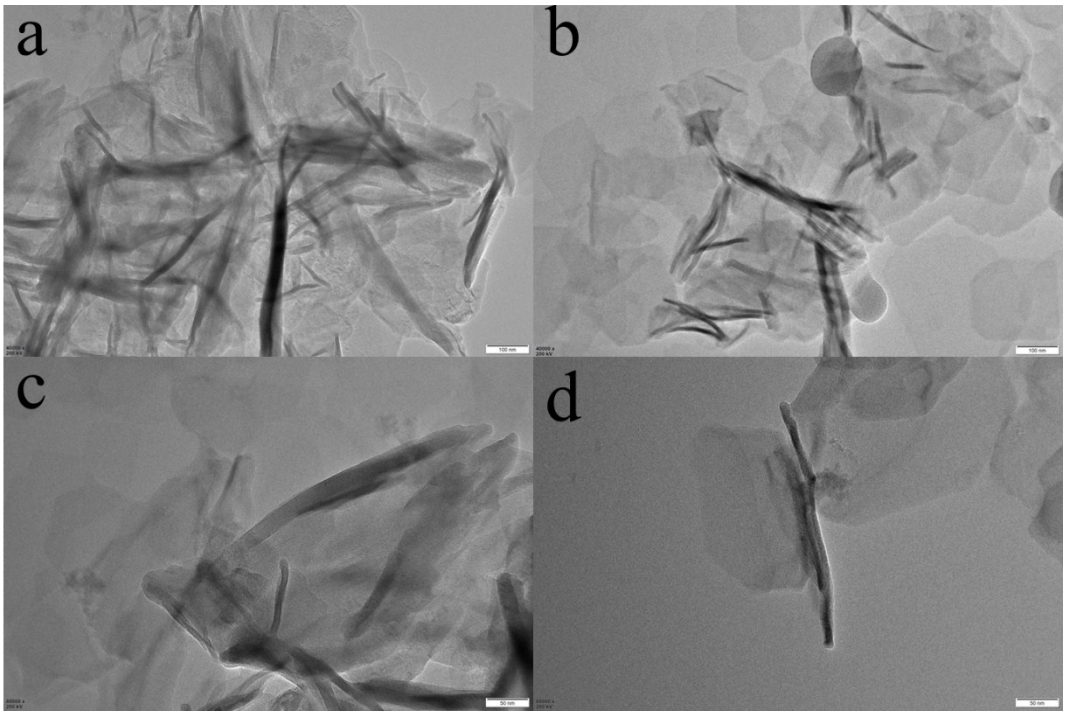

Fig. S8 TEM images of Fe-MOL (Scale bar: (a)100 nm, (b)100 nm, (c)50 nm, (d)50 nm).

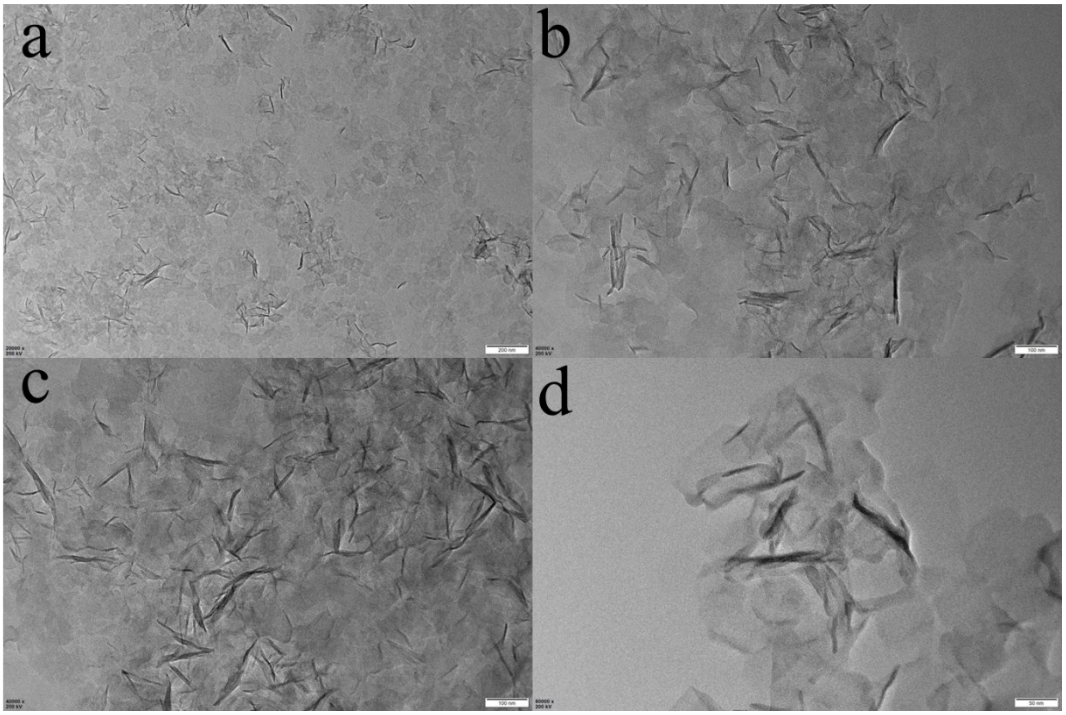

Fig. S9 TEM images of Co-MOL (Scale bar: (a)200 nm, (b)100 nm, (c)100 nm, (d)50 nm).

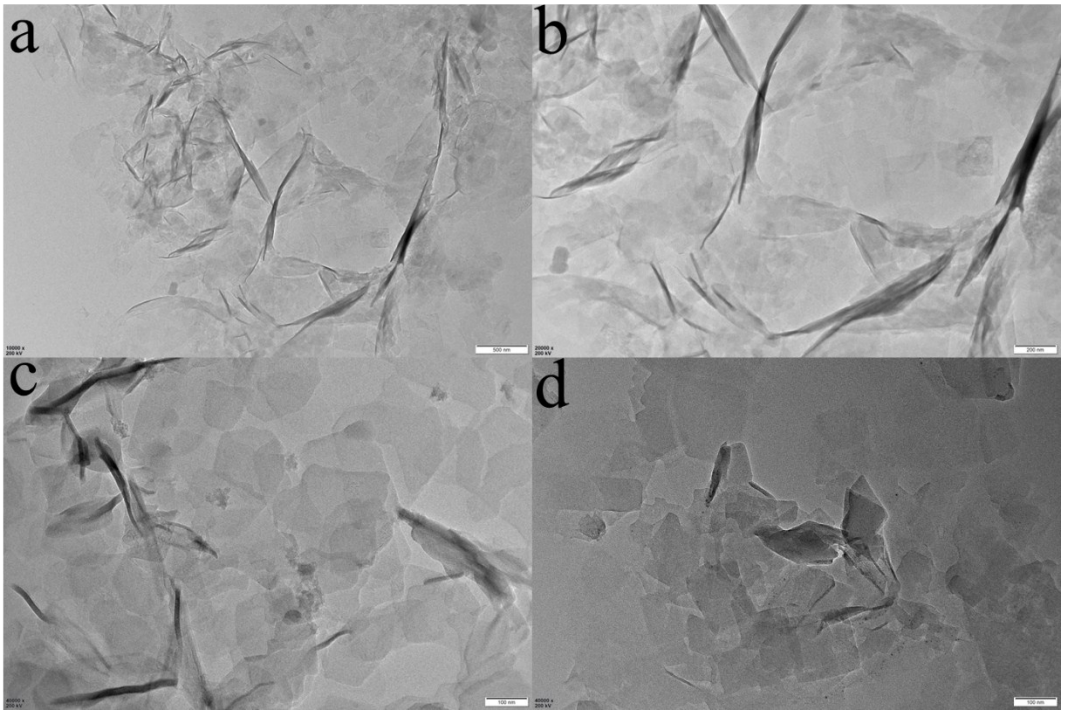

Fig. S10 TEM images of Ni-MOL (Scale bar: (a)500 nm, (b)200 nm, (c)100 nm, (d)100 nm).

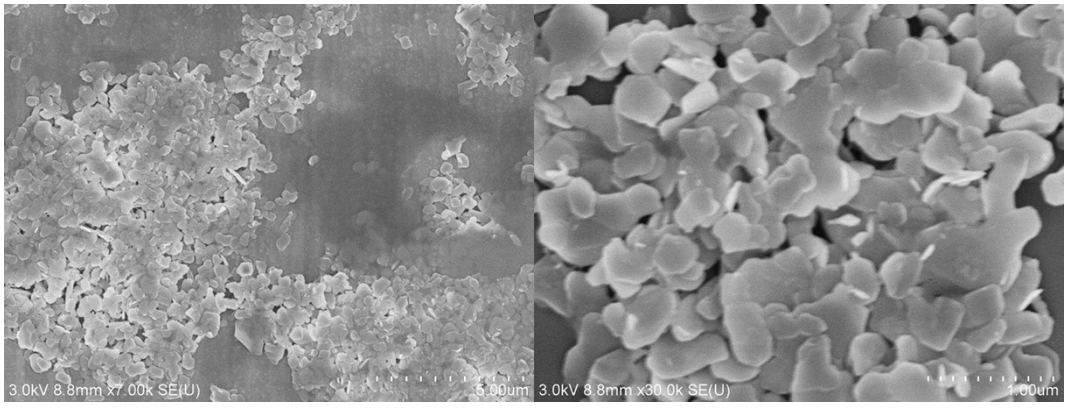

Fig. S11 SEM images of Mn-MOL.

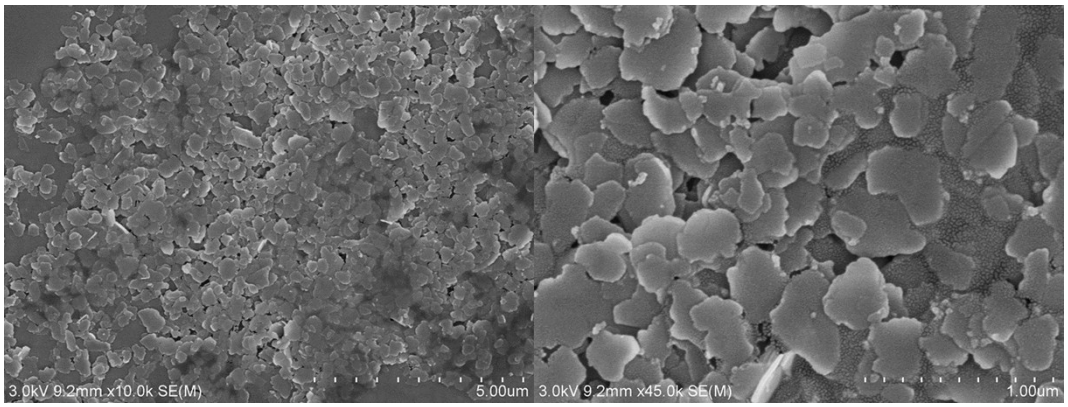

Fig. S12 SEM images of Fe-MOL.

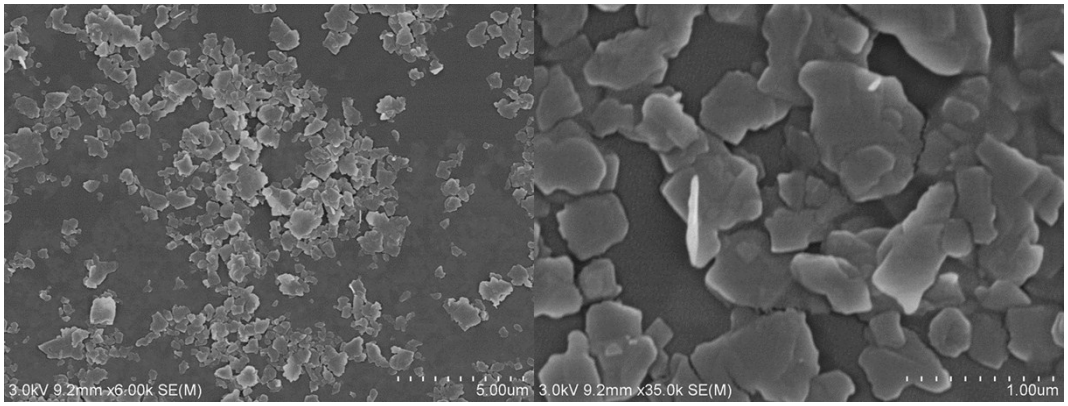

Fig. S13 SEM images of Co-MOL.

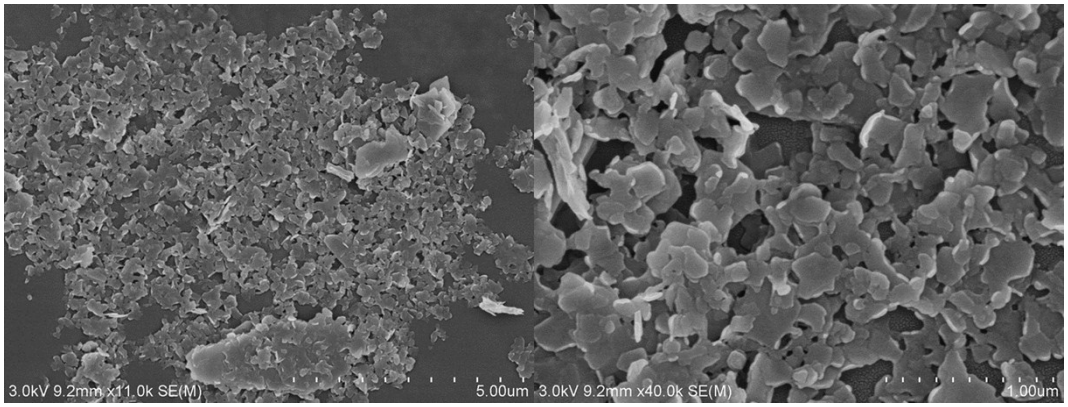

Fig. S14 SEM images of Ni-MOL.

12. FTIR spectra of MOF and MOL

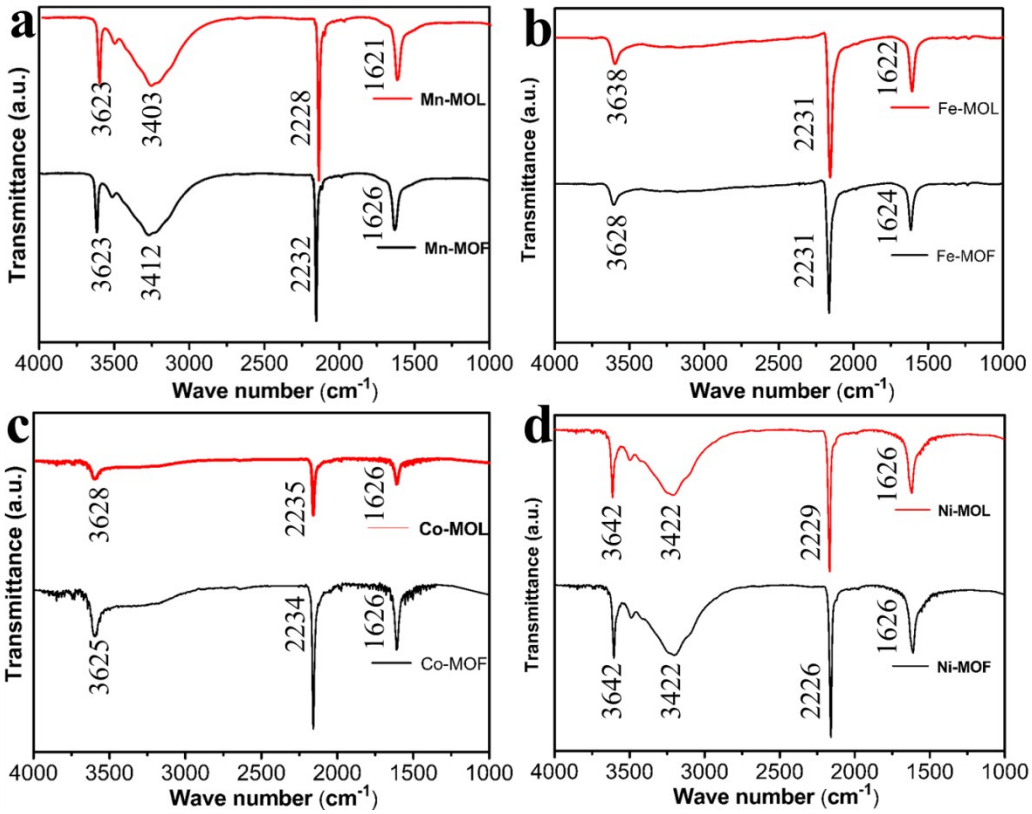

Fig. S15 (a) IR spectra of (a) Mn-MOF and Mn-MOL, (b) Fe-MOF and Fe-MOL, (c) Co-MOF and Co-MOL, and (d) Ni-MOF and Ni-MOL. (The peaks at about 3620 cm^{-1} are due to the OH group, the peaks at about 3400 cm^{-1} are due to water molecular, the peaks at about 2200 cm^{-1} are due to the CN group, the peaks at about 1620 cm^{-1} are due to the bending mode of the water molecular.)

13. XPS spectrum of $Fe(OH)_3$-NS

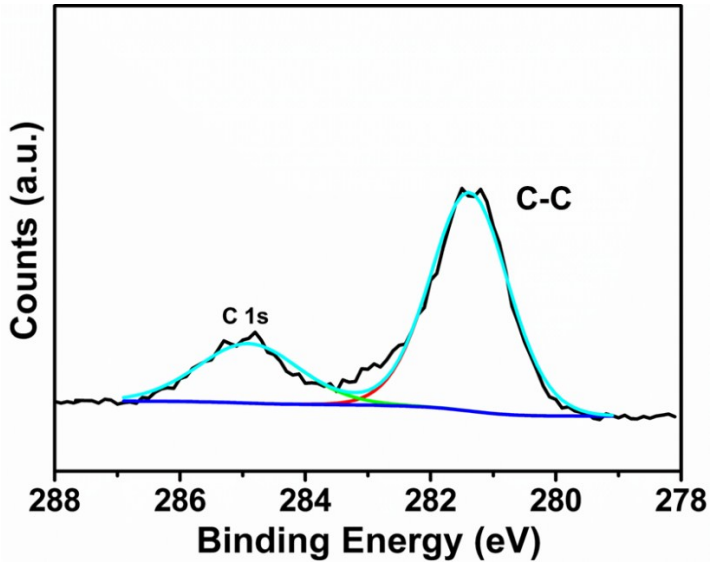

Fig. S16 XPS spectrum of C 1s of $Fe(OH)_3$-NS. The C–C bond originating from carbon contamination.

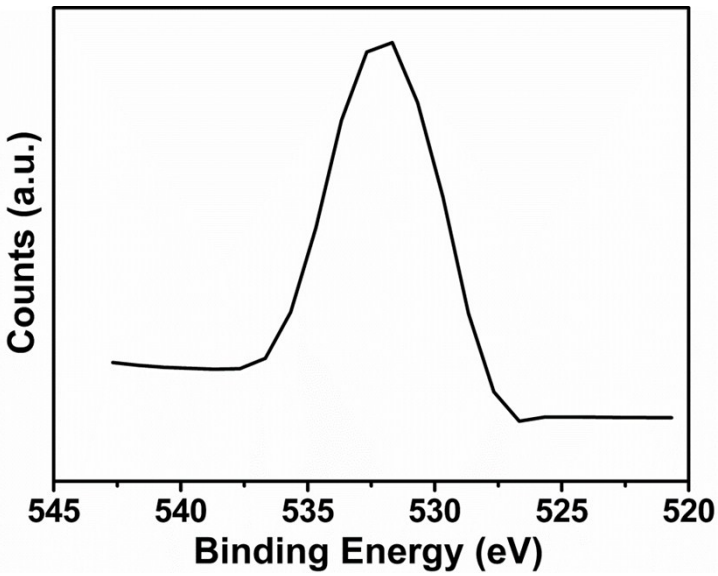

Fig. S17 XPS spectrum of O 1s of $Fe(OH)_3$-NS. The presence of the O 1s peak at 532.23 eV is due to large dominance of –OH species absorbed on the surface by hydroxides.

14. FTIR spectra of metal hydroxide nanosheets

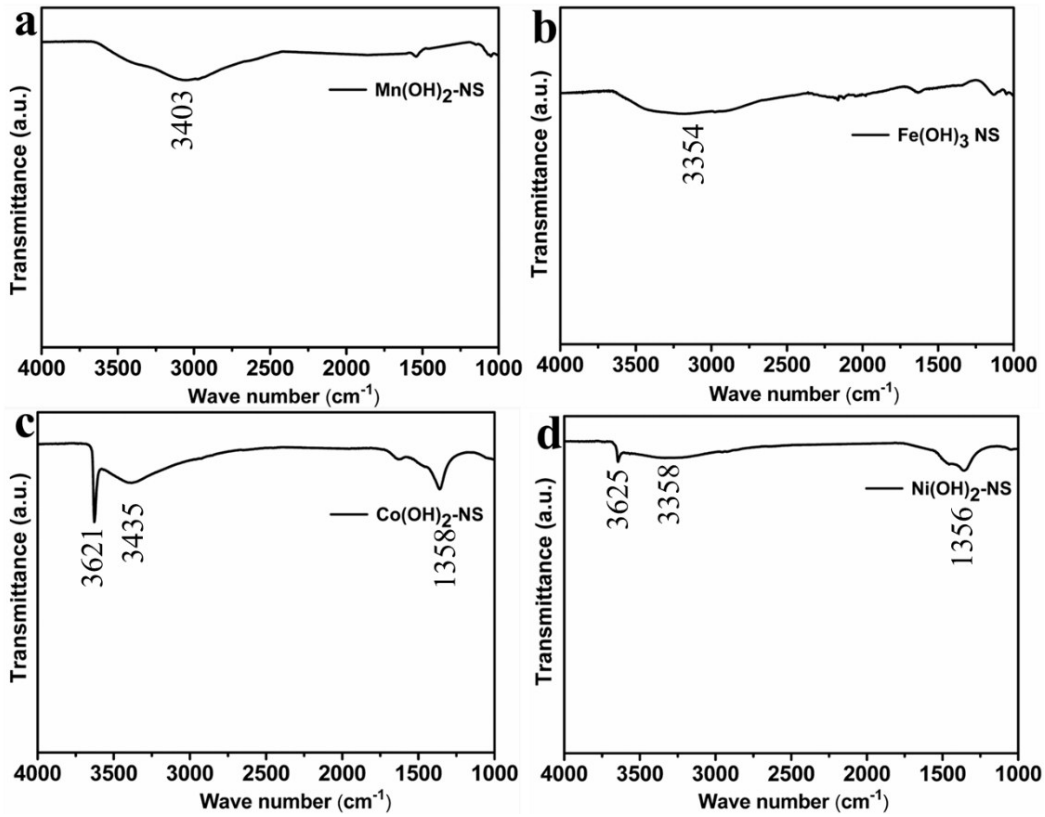

Fig. S18 IR spectra of (a) $Mn(OH)_2$-NS, (b) $Fe(OH)_3$-NS, (c) $Co(OH)_2$-NS, and (d) $Ni(OH)_2$-NS. (The peaks at about 1350 cm^{-1} are due to the CO_3^{2-} from the adsorption of gas phase CO_2.)

15. Tyndall effect images of metal hydroxide nanosheets

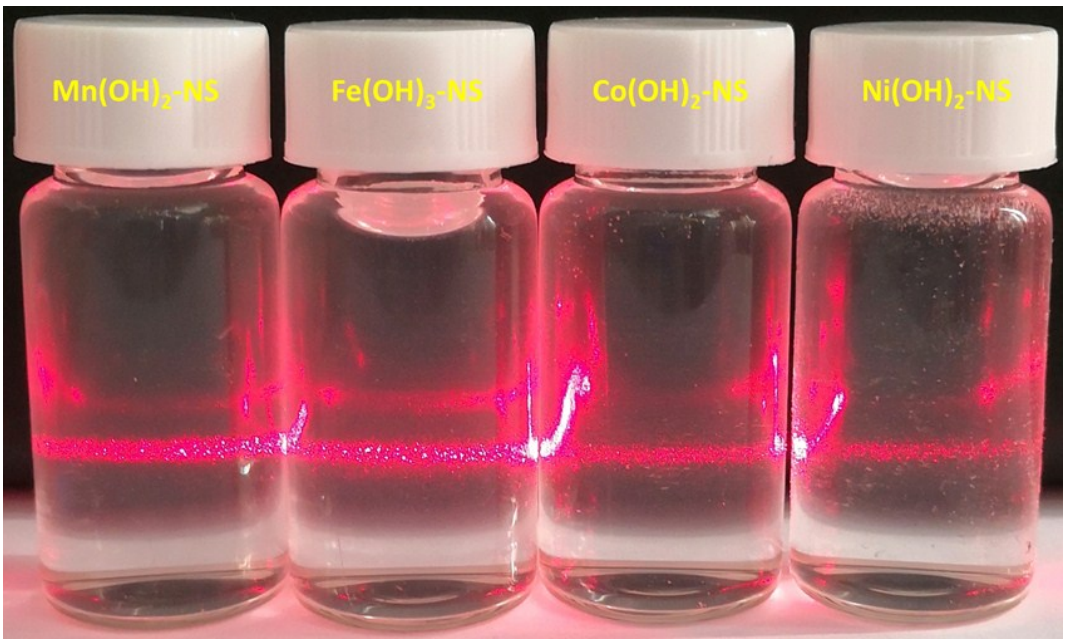

Fig. S19 Tyndall effect images of metal hydroxide nanosheets.

16. XRD patterns of metal hydroxide nanosheets

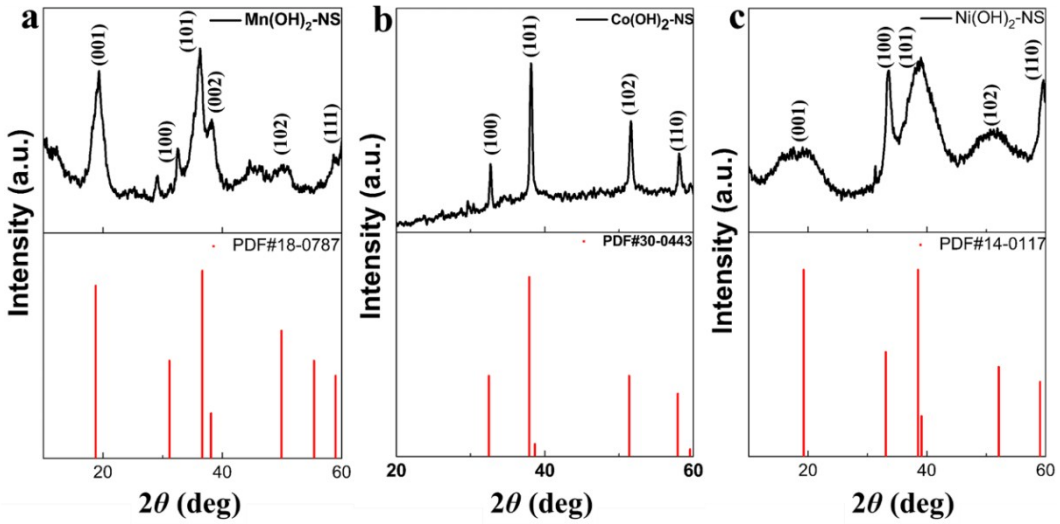

Fig. S20 (a) XRD pattern of $Mn(OH)_2$-NS and $Mn(OH)_2$ (JCPDS no. 18-0787); (b) XRD pattern of $Co(OH)_2$-NS and $Co(OH)_2$ (JCPDS no. 30-0443); (c) XRD pattern of $Ni(OH)_2$-NS and $Ni(OH)_2$ (JCPDS no. 14-0117).

17. SEM images of metal hydroxide nanosheets

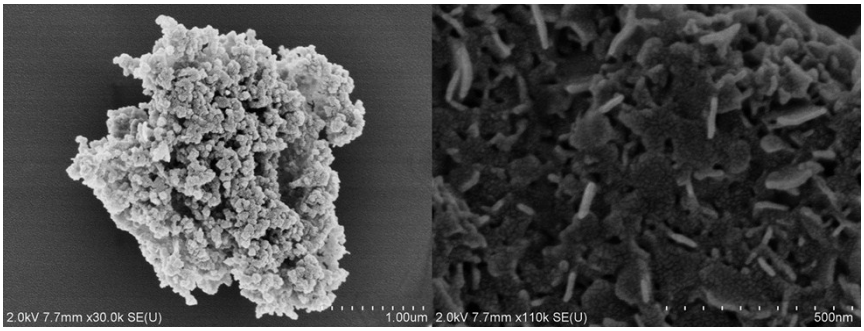

Fig. S21 SEM images of $Mn(OH)_2$-NS.

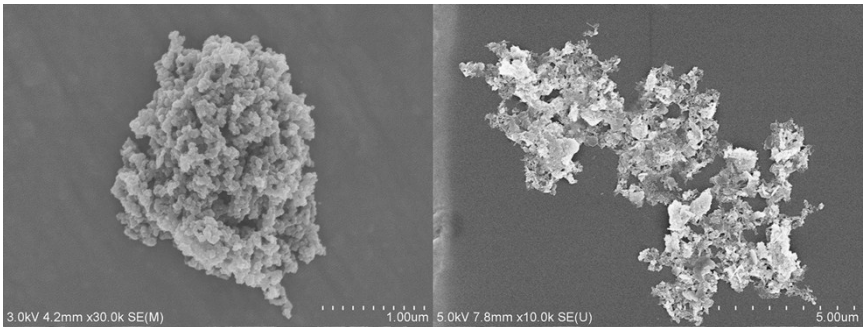

Fig. S22 SEM images of $Fe(OH)_3$-NS.

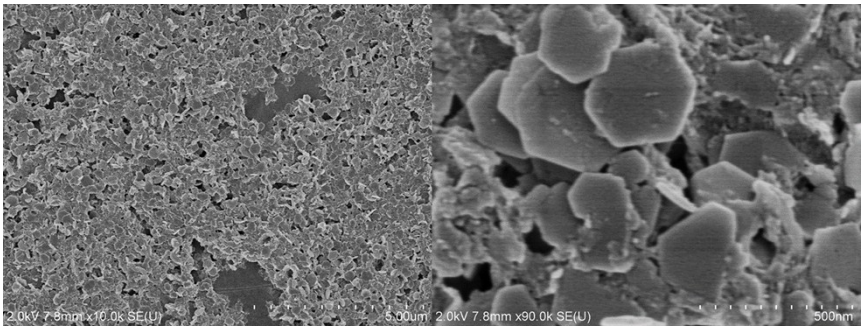

Fig. S23 SEM images of $Co(OH)_2$-NS.

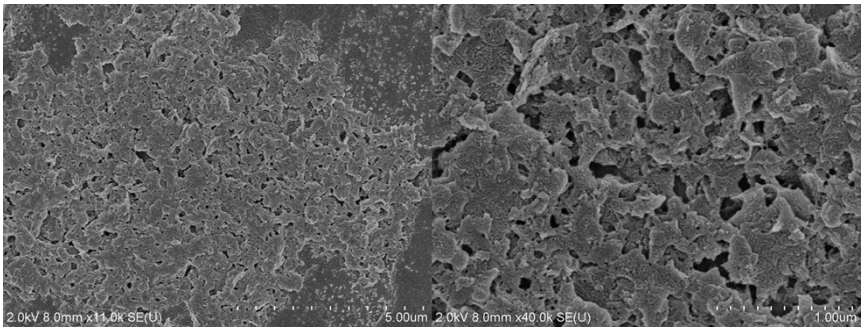

Fig. S24 SEM images of $Ni(OH)_2$-NS.

18. TEM images of metal hydroxide nanosheets

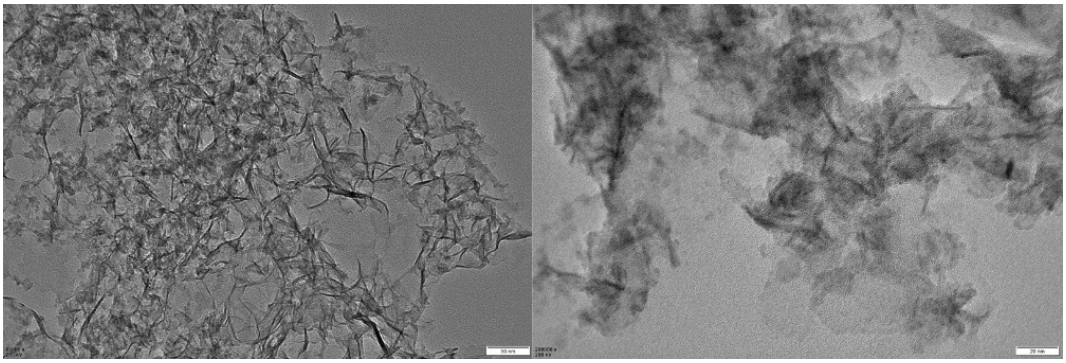

Fig. S25 TEM images of $Mn(OH)_2$-NS (Scale bar: left, 50 nm; right, 20 nm).

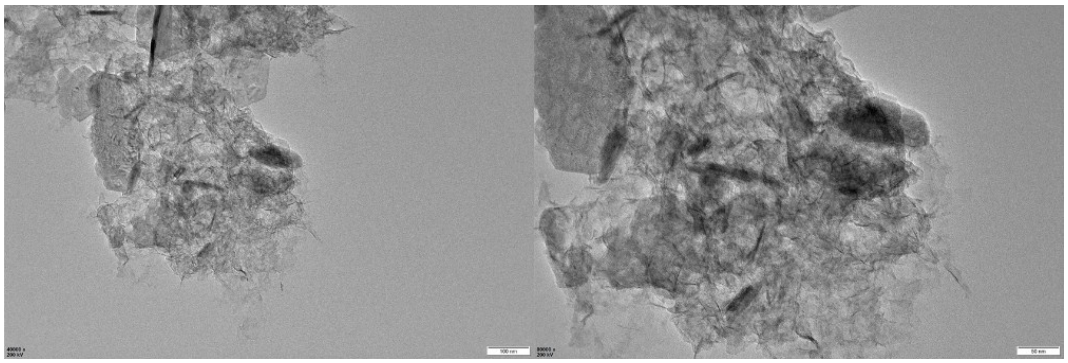

Fig. S26 TEM images of $Co(OH)_2$-NS (Scale bar: left, 100 nm; right, 50 nm).

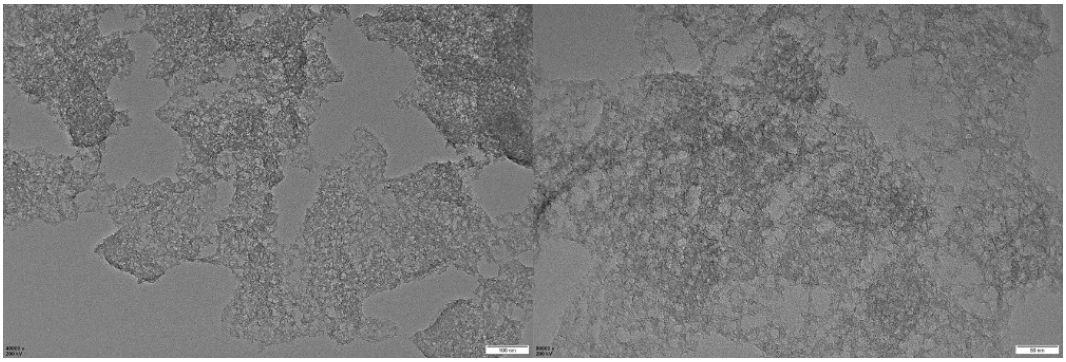

Fig. S27 TEM images of $Ni(OH)_2$-NS (Scale bar: left, 100 nm; right, 50 nm).

19. AFM images of metal hydroxide nanosheets

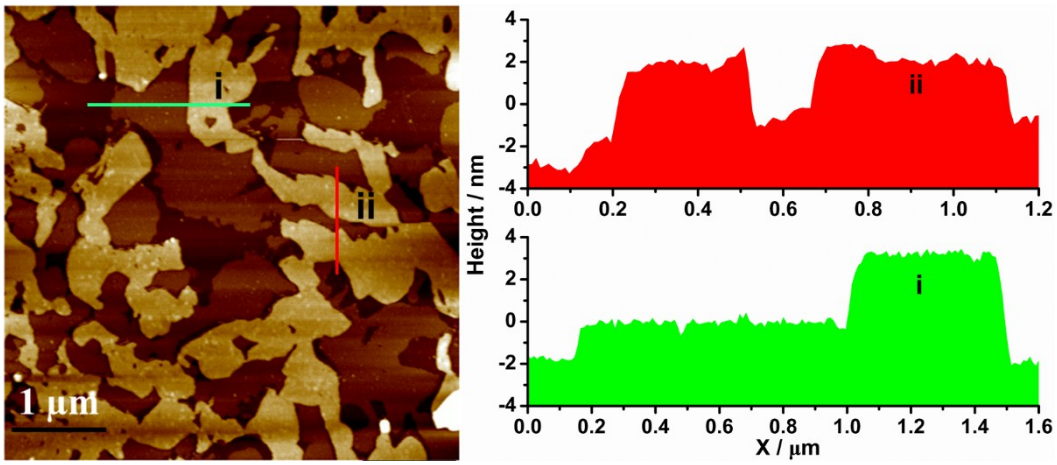

Fig. S28 AFM image of $Mn(OH)_2$-NS with corresponding height profiles of terrace structure.

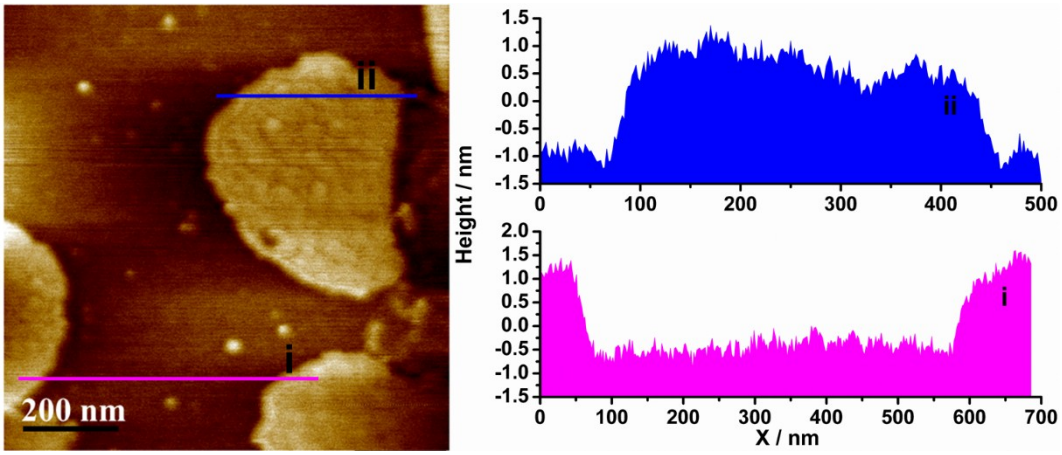

Fig. S29 AFM image of $Co(OH)_2$-NS with corresponding height profiles of terrace structure.

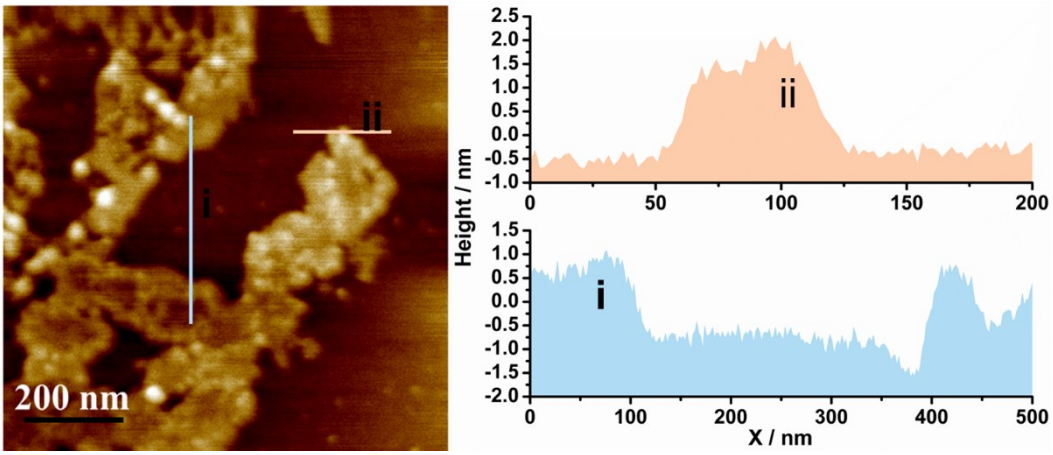

Fig. S30 AFM image of $Ni(OH)_2$-NS with corresponding height profiles of terrace structure.

20. Equivalent circuit

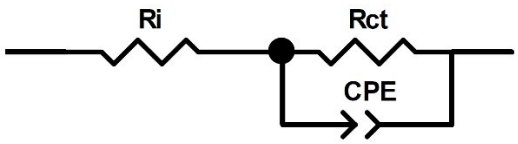

Fig. S31 Equivalent circuit applied for fitting the impedance spectra recorded on the investigated catalysts.

21. Electrochemical data

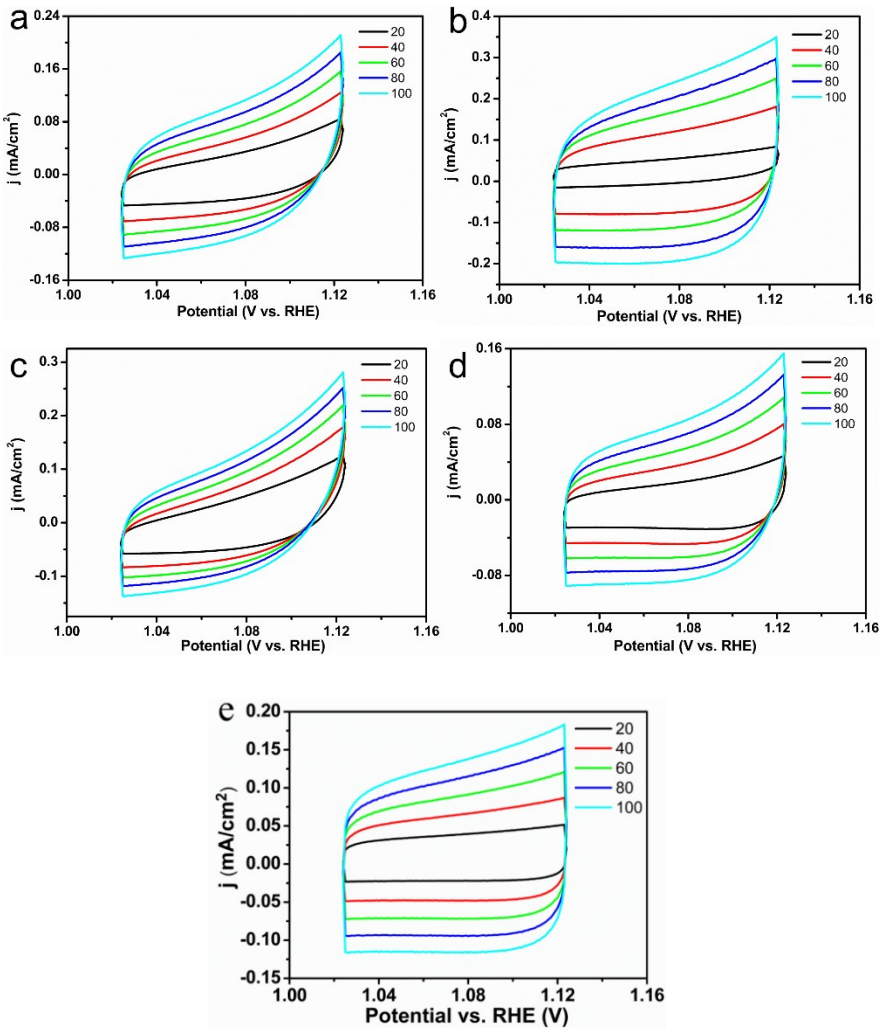

Fig. S32 CV curves in a potential range of 1.02–1.12 V versus RHE: (a) $Mn(OH)_2$-NS, (b) $Fe(OH)_3$-NS, (c) $Co(OH)_2$-NS, (d) $Ni(OH)_2$-NS and (e) NF.

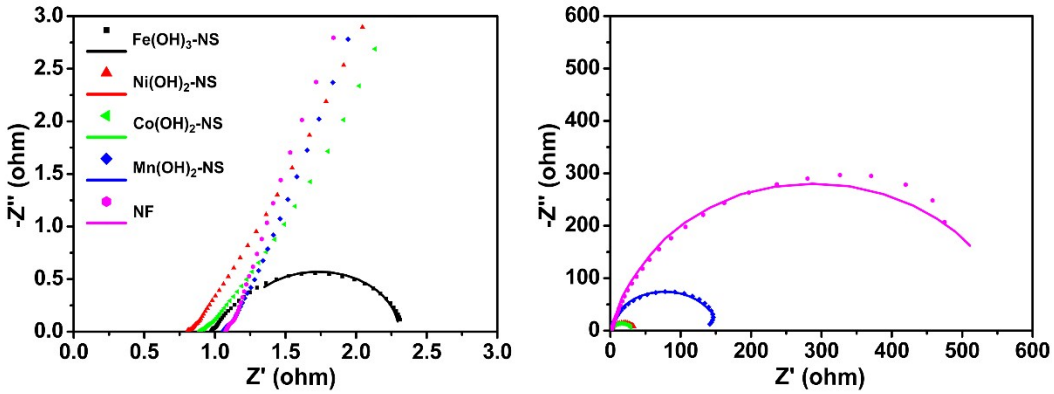

Fig. S33 Nyquist plots of different catalysts with a potential of 1.52 V (vs. RHE), scatter points are experimentally obtained data and solid lines are the fitted curves.

Table S3. Circuit parameters of all catalysts

Name	*R*i (Ω)	*R*ct (Ω)	Q (C)	n
$Mn(OH)_2$-NS	1.02	155.63	0.01027	0.8855
$Fe(OH)_3$-NS	0.99	1.41	0.01744	0.8499
$Co(OH)_2$-NS	0.91	29.12	0.08824	0.8059
$Ni(OH)_2$-NS	0.81	33.26	0.08284	0.8101
NF	1.06	556.38	0.00803	0.8392

Table S4. The turnover frequencies (TOFs) of all the electrocatalysts

Sample	**$Mn(OH)_2$-NS**	**$Fe(OH)_3$-NS**	**$Co(OH)_2$-NS**	**$Ni(OH)_2$-NS**	**IrO_2**
TOF(s^{-1})	$2.1*10^{-3}$	$59.2*10^{-3}$	$3.0*10^{-3}$	$3.3*10^{-3}$	$67.0*10^{-3}$

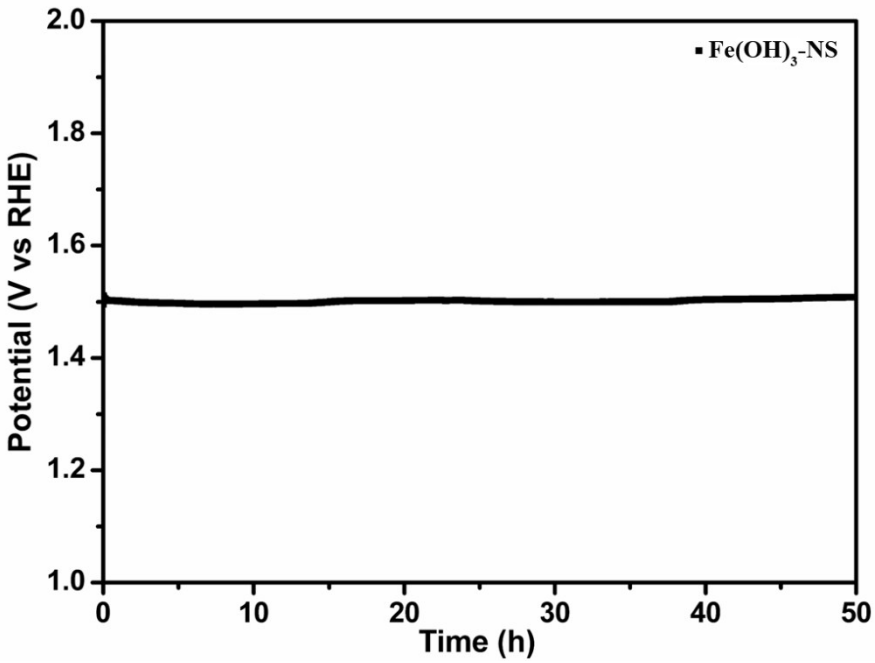

Fig. S34 Chronopotentiometric curve of $Fe(OH)_3$-NS at 10 mA/cm^2.

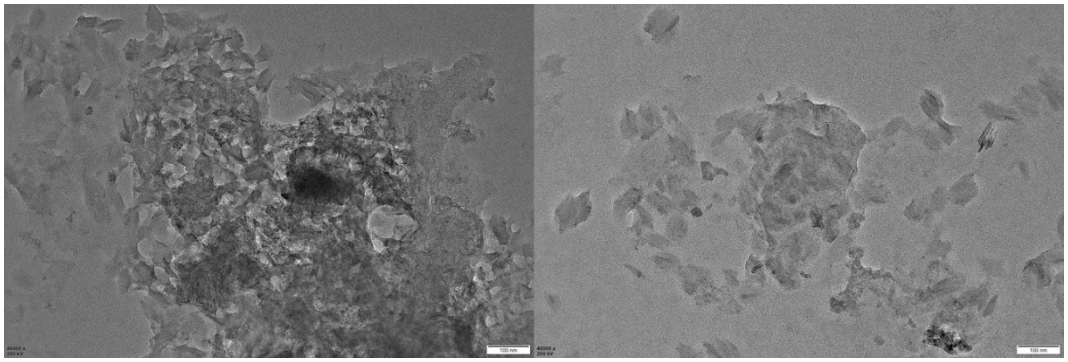

Fig. S35 TEM images of $Fe(OH)_3$-NS after 2000th LSV test.

Table S5. The effect of mass loading on the catalytic activity of $Fe(OH)_3$-NS catalyst

Load quality	0.05 mg/cm^2	0.1 mg/cm^2	0.16 mg/cm^2	0.2 mg/cm^2	0.25 mg/cm^2
η(10 mA cm^{-2})	280 mV	275 mV	271 mV	270 mV	275 mV

Table S6. Electrocatalytic OER performance of Fe-based electrocatalysts

Name	Substrate	η@10 mA cm^{-2}	Tafel slope (mV dec-1)	Stability (h)	Ref.
FeOOH	NF	290	48	11	[4]
FeOOH nanoparticles	NF	290	39	24	[5]
Fe(oxy)hydroxide	Au	350	-	-	[6]
Ni-Fe nanoprisms	NF	295	59	6	[7]
Ni-Fe LDH coupled GO	NF	232	48	8	[8]
Ni-Fe LDH	GC	302	40	3	[9]
FeCo2S4	NF	<270	59	20	[10]
H-Co_9S_8/Fe_3O_4@SNC	GC	280	87	10	[11]
$Co_{0.75}Fe_{0.25}$	GC	303	39	-	[12]
Fe^{2+}-NiFe LDH	CFP	195	-	15	[13]
NiFe LDHs-V_{Ni}	GC	229	63	63	[14]
NiCoFe-NC	GC	250	31	24	[15]
FeS_2/CoS_2 NSs	NF	<300	42	80	[16]
NiFe LDHNiSe/NF	NF	<330	65.6	12	[17]
Co-Fe-1-1	CFP	330	37	20	[18]
$Ni/NiO/Fe_3O_4$	GC	260	62	40	[19]
CoFe/NF	NF	220	40	50	[20]
FeOOH/NiFe	NF	220	-	40	[21]
$Fe(OH)_3$-NS	NF	271	50	50	This work

CFP: carbon fiber paper, GC: glass carbon electrode

22. References

[1] *SAINT-Plus*, version 6.02; Bruker Analytical X-ray System: Madison, WI, 1999.

[2] G. M. Sheldrick, *SADABS An empirical absorption correction program*, Bruker Analytical X-ray Systems: Madison, WI, 1996.

[3] G. M. Sheldrick, *SHELXTL-97*; Universität of Göttingen: Göttingen, Germany, 1997.

[4] P. T. Babar, B. S. Pawar, A. C. Lokhande, M. G. Gang, J. S. Jang, M. P. Suryawanshi, S. M. Pawar and J. H. Kim, *J. Energ. Chem.*, 2017, **26**, 757-761.

[5] J. Lee, H. Lee, B. Lim, *J. Ind. Eng. Chem*., 2018, **58**, 100-104.

[6] S. Zou, M. S. Burke, M. G. Kast, J. Fan, N. Danilovic and S. W. Boettcher, *Chem. Mater.*, 2015, **27**, 8011-8020.

[7] L. Yu, J. F. Yang, B. Y. Guan, Y. Lu and X. W. Lou, *Angew. Chem., Int. Ed.* 2018, **57**, 172-176.

[8] X. Long, J. Li, S. Xiao, K. Yan, Z. Wang, H. Chen and S, Yang, *Angew. Chem*., *Int. Ed.* 2014, **53**, 7584-7588.

[9] F. Song and X. Hu, *Nat. Chem.*, 2014, **5**, 4477.

[10] J. Hu, Y. Ou, Y. Li, D. Gao, Y. Zhang, and P. Xiao, *ACS Sustainable Chem. Eng.,* 2018, **6**, 11724−11733.

[11] L. Gan, J. Fang, M. Wang, L. Hu, K. Zhang, Y. Lai and J. Li, *J. Power Sources.,* 2018, **391**, 59–66.

[12] X. Feng, X. Bo and L. Guo, *J. Power Sources.,* 2018, **389,** 249–259.

[13] Z. Cai, D. Zhou, M. Wang, S.-M. Bak, Y. Wu, Z. Wu, Y. Tian, X. Xiong, Y. Li, W. Liu, S. Siahrostami, Y. Kuang, X.-Q. Yang, H. Duan, Z. Feng, H. Wang and X. Sun, *Angew. Chem., Int. Ed.* 2018, **57**, 9392 –9396.

[14] Y. Wang, M. Qiao, Y. Li, S. Wang, *Small,* 2018, **14**, 1800136

[15] W. Liu, X. Hu, H. Li and H. Yu, *Small,* 2018, **14**, 1801878.

[16] Y. Li, J. Yin, L. An, M. Lu, K. Sun, Y. Zhao, D. Gao, F. Cheng and P. Xi, *Small,* 2018, **14**, 1801070.

[17] S. Dutta, A. Indra, Y. Feng, T. Song, and U. Paik, *ACS Appl. Mater. Interfaces.,* 2017, **9**, 33766−33774.

[18] M. Xiong and D. Ivey, *Electrochimi Acta.,* 2018, **260**, 872-881.

[19] Y. Xie, X.Wang, K. Tang, Q. Li, and C.Yan, *Electrochimi Acta.,* 2018, **264** 225-232.

[20] P. Babar, A. Lokhande, H. Shin, B. Pawar, M. Gang, S. Pawar and J. Kim, *Small,* 2018, **14**, 1702568.

[21] J. Chi, H. Yu, G. Jiang, J. Jia, B. Qin, B. Yi and Z. Shao, *J. Mater. Chem. A.,* 2018, **6**, 3397–3401.